INTERNATIONAL JOURNAL FOR NUMERICAL METHODS IN FLUIDS, VOL. 9, 1503–1516 (1989)

MARANGONI CONVECTION IN WELD POOLS WITH A FREE SURFACE

M. C. TSAI AND SINDO KOU

Center of Excellence in Solidification Processing Technologies of Engineering Materials and Department of Materials Science and Engineering, University of Wisconsin, 1509 University Avenue, Madison, WI 53706, U.S.A.

SUMMARY

A steady-state two-dimensional model of heat transfer and fluid flow was developed to describe Marangoni convection in the weld pool. Both the pool surface and the fusion boundary were calculated. The validity of the model was verified against an asymptotic solution for Marangoni-convection-induced free surface geometry. Two different cases were studied, i.e. a negative surface tension temperature coefficient $\partial\gamma/\partial T$ and a positive one, and the resultant shapes of the weld pool surface were compared.

KEY WORDS Welding Free surface Marangoni convection

INTRODUCTION

In fusion welding the heat source causes a small portion of the workpiece material to melt and creates a small pool of molten metal, i.e. the weld pool. Heat transfer and fluid flow in the weld pool can significantly affect the microstructure and properties of the resultant weld. So far most of the models for heat transfer and fluid flow in weld pools have been based on the 'rigid-lid' assumption, i.e. the weld pool surface is flat and is undeformable.[1–18] Recently, Zacharia *et al.*[19,20] have relaxed this assumption and calculated heat transfer and fluid flow in arc weld pools using rectangular co-ordinates. The surface geometry of a deformed laser weld pool had been shown in an earlier study by Chan *et al.*[10] However, nothing was mentioned about how the result was obtained, though in the same study rectangular co-ordinates were used for calculating Marangoni (i.e. surface-tension-driven) convection in weld pools with a flat, undeformable surface. Paul and DebRoy[21] have also studied the deformation of a laser weld pool due to Marangoni convection using rectangular co-ordinates. Recently, McLay and Carey[22] have used the finite element method to calculate heat transfer and fluid flow in a weld pool. The shapes of the deformed pool surface and the pool bottom, which were specified rather than calculated, were closely fitted by finite element grids.

The disadvantages of rectangular and cylindrical co-ordinates for calculating weld pool deformation have been described recently by Tsai and Kou,[23] i.e. the boundary conditions at the weld pool surface and hence its deformation cannot be treated properly. Specifically, since neither co-ordinates can fit well the free surface of a deformed weld pool, the surface-tension-induced normal and shear stresses are difficult to handle. Consequently, the shape of the free surface and the surface-tension-induced flow at and immediately below the free surface, where it is most significant, cannot be calculated properly. It should be pointed out that the paper of Tsai and Kou[23] emphasized the advantages of orthogonal curvilinear co-ordinates in treating a free surface

0271–2091/89/121503–14$07.00

Received 18 July 1988
Revised 27 January 1989

problem involving the weld pool. However, it did not touch upon the main subjects of the present paper, i.e. the numerical methods (for heat transfer, fluid flow and surface deformation), the effect of the surface tension temperature coefficient $\partial\gamma/\partial T$, how deformed and undeformed weld pools differ from each other in their velocity and temperature profiles, and comparison of the model against an asymptotic solution.

The purpose of the present paper is to study Marangoni convection in weld pools with a free, deformable surface and the resultant shape or deformation of the pool surface. Since this type of deformation can be better studied without the presence of other deformation-causing factors (e.g. the arc pressure), Marangoni convection alone will be considered here. Weld pool deformation caused by other factors will be presented elsewhere. The workpiece material to be considered here is 6061 aluminium alloy, which is essentially aluminium with about 0·6 wt% Si and 1·0 wt% Mg.

MATHEMATICAL FORMULATION

A schematic sketch of the physical system is shown in Figure 1. The free surface is the surface of the weld pool, while the pool (fusion) boundary is the liquidus isotherm (T_L) in the case of an alloy and the melting point in the case of a pure metal. Since our model is intended for various materials, including those with temperature-dependent thermal properties, it is impractical to use dimensionless variables. As such, the governing equations and boundary conditions will be presented in dimensional forms.

The problem here involves two free boundaries—one is the weld pool surface and the other the pool boundary. Since the first free boundary is more critical and more difficult to handle, we choose to fit it, rather than the second one, with orthogonal curvilinear co-ordinates.

The equation of continuity for axisymmetric orthogonal curvilinear co-ordinates η and ξ is

$$\frac{\rho}{h_1 h_2 r}\left(\frac{\partial}{\partial\eta}(h_2 r u)+\frac{\partial}{\partial\xi}(h_1 r w)\right)=0, \tag{1}$$

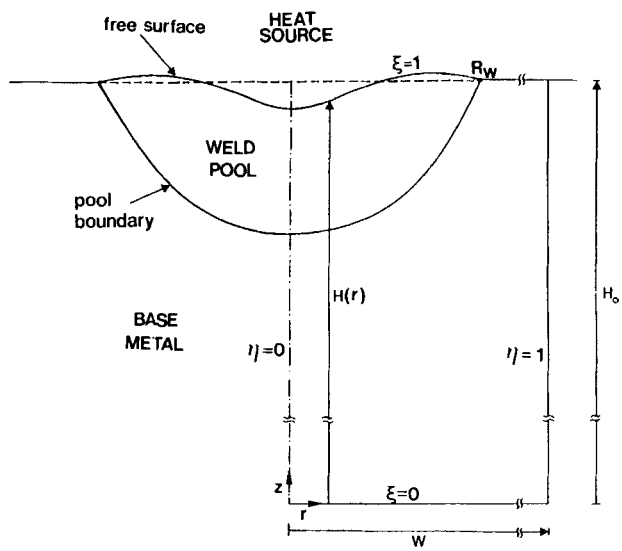

Figure 1. Schematic illustration of weld pool deformation and the co-ordinates used for calculating heat transfer and fluid flow in the weld pool.

where h_1 and h_2 are the metric coefficients for the η- and ξ-co-ordinates respectively, r is the radial distance, u and w are the velocity components in the η- and ξ-directions respectively and ρ is the density. The grid system is set up so that the curve of $\xi = 1$ fits the weld pool surface, while the straight line of $\eta = 0$ fits the centreline of the pool and the unmelted workpiece, i.e. the base metal.

The η- and ξ-components of the equation of motion are[24]

$$\frac{\rho}{h_1 h_2 r}\left(\frac{\partial}{\partial \eta}(h_2 r u^2)+\frac{\partial}{\partial \xi}(h_1 r u w)\right)=-\frac{1}{h_1}\frac{\partial P}{\partial \eta}+\frac{1}{h_1 h_2 r}\left(\frac{\partial}{\partial \eta}(h_2 r \sigma_{11})+\frac{\partial}{\partial \xi}(h_1 r \sigma_{21})\right)$$
$$+\frac{\sigma_{12}}{h_1 h_2}\frac{\partial h_1}{\partial \xi}-\frac{\sigma_{22}}{h_1 h_2}\frac{\partial h_2}{\partial \eta}+\frac{\rho w^2}{h_1 h_2}\frac{\partial h_2}{\partial \eta}-\frac{\rho u w}{h_1 h_2}\frac{\partial h_1}{\partial \xi}-\frac{\sigma_{33}}{h_1 r}\frac{\partial r}{\partial \eta}+\rho g_\eta, \quad (2)$$

$$\frac{\rho}{h_1 h_2 r}\left(\frac{\partial}{\partial \eta}(h_2 r u w)+\frac{\partial}{\partial \xi}(h_1 r w^2)\right)=-\frac{1}{h_2}\frac{\partial P}{\partial \xi}+\frac{1}{h_1 h_2 r}\left(\frac{\partial}{\partial \eta}(h_2 r \sigma_{12})+\frac{\partial}{\partial \xi}(h_1 r \sigma_{22})\right)$$
$$+\frac{\sigma_{21}}{h_1 h_2}\frac{\partial h_2}{\partial \eta}-\frac{\sigma_{11}}{h_1 h_2}\frac{\partial h_1}{\partial \xi}+\frac{\rho u^2}{h_1 h_2}\frac{\partial h_1}{\partial \xi}-\frac{\rho u w}{h_1 h_2}\frac{\partial h_2}{\partial \eta}-\frac{\sigma_{33}}{h_2 r}\frac{\partial r}{\partial \xi}+\rho g_\xi, \quad (3)$$

where the components of the stress tensor $\sigma_{i,j}$ are

$$\sigma_{11}=2\mu\left(\frac{1}{h_1}\frac{\partial u}{\partial \eta}+\frac{w}{h_1 h_2}\frac{\partial h_1}{\partial \xi}\right),$$
$$\sigma_{22}=2\mu\left(\frac{1}{h_2}\frac{\partial w}{\partial \xi}+\frac{u}{h_1 h_2}\frac{\partial h_2}{\partial \eta}\right),$$
$$\sigma_{21}=\sigma_{12}=\mu\left[\frac{h_2}{h_1}\frac{\partial}{\partial \eta}\left(\frac{w}{h_2}\right)+\frac{h_1}{h_2}\frac{\partial}{\partial \xi}\left(\frac{u}{h_1}\right)\right],$$
$$\sigma_{33}=2\mu\left(\frac{u}{h_1 r}\frac{\partial r}{\partial \eta}+\frac{w}{h_2 r}\frac{\partial r}{\partial \xi}\right),$$

and g_η and g_ξ are the η- and ξ-components of the gravitational acceleration **g**.

The equation of energy is

$$\frac{\rho}{h_1 h_2 r}\left(\frac{\partial}{\partial \eta}(h_2 r u H)+\frac{\partial}{\partial \xi}(h_1 r w H)\right)=\frac{1}{h_1 h_2 r}\left[\frac{\partial}{\partial \eta}\left(\frac{h_2 r}{h_1}k\frac{\partial T}{\partial \eta}\right)+\frac{\partial}{\partial \xi}\left(\frac{h_1 r}{h_2}k\frac{\partial T}{\partial \xi}\right)\right], \quad (4)$$

where H is the enthalpy, k is the thermal conductivity and T is the temperature. The use of the enthalpy H in equation (4) allows the heat of fusion to be considered while the position of the pool boundary is being determined in the heat flow calculation. This is the so-called 'enthalpy method'. The Boussinesq approximation was used with a thermal expansion coefficient $\beta_T = 1{\cdot}0 \times 10^{-4}\ ^\circ\mathrm{C}^{-1}$.

The boundary conditions for fluid flow are as follows.

1. At the weld centreline ($\eta = 0$),

$$u=0 \quad \text{and} \quad \sigma_{12}=0.$$

2. At the free surface ($\xi = 1$),[25]

$$w=0,$$
$$\sigma_{21}=\frac{\partial T}{h_1 \partial \eta}\frac{\partial \gamma}{\partial T}+\frac{\partial C}{h_1 \partial \eta}\frac{\partial \gamma}{\partial C}, \quad (5)$$

$$P_a+\sigma_{22}-P+C_1=-\gamma\left(\frac{h''}{(1+h'^2)^{3/2}}+\frac{h'}{r(1+h'^2)^{1/2}}\right) \text{ with}$$

$$h'(0)=h(R_w)=0 \quad \text{and} \quad h=H_0-H(r), \tag{6}$$

where σ_{21} is the shear stress, C is the concentration of the surface-active agent, σ_{22} is the normal stress, P_a is the ambient pressure, P is the pressure from the equation of motion, h is the local weld pool depression and r is the radial distance; h'' and h' are the second and first derivatives of h with respect to r respectively. The constant C_1, which is a reference pressure, is determined from the following constraint of constant volume:

$$2\pi\int_0^{R_w} rh\,dr=0, \tag{7}$$

where R_w is the radius of the weld pool surface.

It should be pointed out that variations in the surface tension due to spatial variations of the concentration of the surface-active agent, i.e. the second term on the RHS of equation (5), will not be considered here. This, for instance, can be caused by evaporation of the surface-active agent.

3. At the weld pool boundary ($T=T_L$),

$$u=w=0.$$

The pool boundary is approximated by small steps of finite difference grid that are closest to the interface, and both u and w are set to zero along these steps. It should be pointed out that in our previous work[4-8] an effective viscosity much higher than the viscosity of the liquid metal was used for the solid metal to reduce both u and w to zero (originally suggested by Patankar[26]). However, since u and w were always set equal to zero wherever $T\leq T_L$, the discontinuity in the viscosity did not actually enter the computation process. In fact, this effective viscosity approach leads to exactly the same condition of $u=w=0$ at the weld pool boundary as in the present case. The non-orthogonal grids used by Craine[16] and Kanouff[18] fit the pool boundary and hence allow this boundary condition to be handled more accurately. The free surface of the weld pool, however, was assumed flat and underformable in both studies.

The boundary conditions for heat transfer, on the other hand, are as follows.

1. At the weld centreline ($\eta=0$),

$$\frac{1}{h_1}\frac{\partial T}{\partial \eta}=0.$$

2. At the free surface ($\xi=1$),

$$-\frac{k}{h_2}\frac{\partial T}{\partial \xi}=\begin{cases}-(3Q/\pi a^2)\exp(-3r^2/a^2), & r\leq a,\\ h_c(T-T_a)+\sigma e(T^4-T_a^4), & r>a,\end{cases}$$

where Q is the power delivered from the arc to the workpiece, a is the effective radius of the arc, h_c is the heat transfer coefficient, T_a is the ambient temperature, σ is the Stefan–Boltzman constant and e is the emissivity. For aluminium alloys the emissivity e ranges from 0·04 for shiny surfaces to 0·19 for heavily oxidized surfaces,[27] and the heat transfer coefficient h_c is approximately 8·5 W m^{-2} °C^{-1}.[28] Because of the low melting point and high thermal conductivity of aluminium, the surface heat loss is usually small and can be neglected. It should be pointed out here that the Gaussian approximation of the heat flux is not valid for large surface deformations, as pointed out by Lin and Eagar.[29] Although any other type of

heat flux distribution can be used in the model, the Gaussian one is still used here in view of the relatively small surface deformations involved.

3. Far away from the centreline ($\eta = 1$),

$$T = T_1(z)$$

4. Far below the free surface ($\xi = 0$),

$$T = T_0(r).$$

METHOD OF SOLUTION

Regarding the last two boundary conditions for heat flow, temperatures $T_1(z)$ and $T_0(r)$ were obtained from the point-heat-source analytical solution of Rosenthal.[30] This solution, though less accurate near the position of the point source because of singularity, is in fact quite accurate in the region sufficiently far away from it. For the small heat input (1800 W) in the semi-infinite workpiece used in the present study, we found $W = 10$ mm and $H_0 = 18$ mm to be sufficient—further increase in these values resulted in no significant changes. For these values of W and H_0, $T_1(z)$ varies from 205 to 107 °C while $T_0(r)$ varies from 118 to 107 °C.

Regarding the enthalpy model, in the solid and liquid phases the enthalpy is related to the temperature through the specific heat of solid, C_S, and the specific heat of liquid, C_L, respectively. In the two-phase region of solid plus liquid (i.e. the so-called mushy zone) the enthalpy can be expressed as $H = H_S(1 - f_L) + H_L f_L$ as an approximation, where H_S, H_L and f_L are the enthalpy of the solid phase at the solidus temperature T_S, the enthalpy of the liquid phase at the liquidus temperature T_L and the fraction of the liquid phase respectively. The liquid fraction f_L is a function of temperature as described, for example, by the Scheil equation.[31] For materials with small amounts of alloying elements, such as 6061 aluminium, the liquid fraction f_L can be approximated as a linear function of temperature varying from zero at T_S to unity at T_L, and H_L can be approximated as $H_S + \Delta H$, where ΔH is the heat of fusion for pure aluminium.

Equations (1)–(4) were solved using the SIMPLE algorithm with the hybrid scheme to help reduce false diffusion.[26] Weighted (i.e. based on the lever-arm rule), rather than central, three-point differencing was used to minimize errors caused by non-uniform grid spacing. The application of the SIMPLE algorithm to weld pool convection has been described elsewhere[4] and hence will not be repeated here. The physical properties of 6061 aluminium alloy, i.e. the workpiece material, used in the calculation are shown in Table I.

The orthogonal curvilinear co-ordinates in Figure 2 were generated numerically by solving co-ordinate transformation equations.[32] The grids were staggered as illustrated in Figure 2. Briefly, the velocity components u and w were calculated at cell boundaries, while all other variables were calculated at the cell centres (denoted by the dots). It should be pointed out that after finishing the computations, u and w were combined and the resultant velocity vectors (V) shown at the cell centres.

Table I. Physical properties of 6061 aluminium alloy[5]

$\beta_T = 1{\cdot}0 \times 10^{-4}\,°C^{-1}$	$\rho = 2700\ kg\,m^{-3}$
$\partial\gamma/\partial T = -0{\cdot}35 \times 10^{-3}\ kg\,s^{-2}\,°C^{-1}$	$C_S = 1066\ J\,kg\,°C^{-1}$
$T_L = 652\,°C$	$C_L = 1066\ J\,kg^{-1}\,°C^{-1}$
$T_S = 582\,°C$	$k_S = 168\ W\,m^{-1}\,°C^{-1}$
$T_a = 25\,°C$	$k_L = 108\ W\,m^{-1}\,°C^{-1}$
$\Delta H = 3{\cdot}95 \times 10^5\ J\,kg^{-1}$	$\mu = 1{\cdot}0 \times 10^{-3}\ kg\,m^{-1}\,s^{-1}$

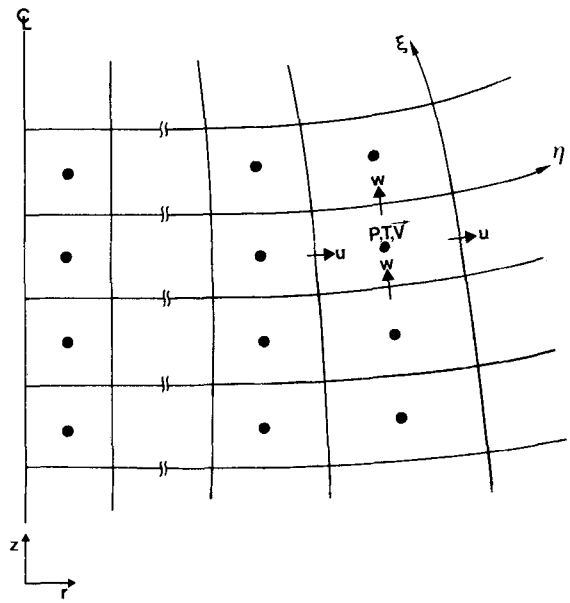

Figure 2. Staggered grid used for computation

At the beginning the weld pool surface was assumed flat, and heat flow and convection were calculated by solving equations (1)–(4) with their proper boundary conditions until the following convergence criteria were met:

$$\frac{\sum|\phi^{\text{new}}-\phi^{\text{old}}|}{\sum|\phi^{\text{new}}|}\leq 10^{-3} \qquad \text{for velocities and pressure,}$$

$$|T^{\text{new}}-T^{\text{old}}|_{\max}\leq 1\,^{\circ}\text{C} \qquad \text{for temperature,}$$

where $\sum$ denotes summation over all grid points, ϕ denotes u, w or P, and 'max' denotes the maximum value of all grid points. The calculated results did not change significantly beyond these criteria.

Then, with the temperature and velocity fields so obtained, an initial guess for C_1 was made, equation (6) was solved by the multiple-shooting method or Runge–Kutta method, and the LHS of equation (7) was computed by Simpson's rule.[33] The false position method was used to get a new C_1, and the whole procedure was repeated until the following convergence criterion was met:

$$|C_1^{\text{new}}-C_1^{\text{old}}|\leq 10^{-9}.$$

This usually insured that the LHS of equation (7) became less than 10^{-17}. In this way, the new free surface was determined and a new grid could now be generated by solving co-ordinate transformation equations with the following convergence criteria:

$$\left|\frac{\psi^{\text{new}}-\psi^{\text{old}}}{\psi^{\text{new}}}\right|_{\max}\leq 10^{-6} \qquad \text{for } r \text{ and } z,$$

$$\left|\frac{\partial r}{\partial \eta}\frac{\partial r}{\partial \xi}+\frac{\partial z}{\partial \eta}\frac{\partial z}{\partial \xi}\right|_{\max}\leq 10^{-6} \qquad \text{for the orthogonality requirement,}$$

where ψ stands for r or z.

The whole procedure mentioned above was repeated until the following convergence criterion was met:

$$|h^{new} - h^{old}|_{max} \leq 10^{-7}.$$

A Harris 800 main frame computer was used to carry out the computations and the CPU times were of the order of 100 min.

RESULTS AND DISCUSSION

Comparison with asymptotic solution

Since no analytical solutions are known to us for checking the validity of our method of solution, it was checked against the asymptotic solution of Sen and David[34] for surface deformation produced by Marangoni convection in a liquid contained in a rectangular slot. In order to do this, our computer program was modified so that the two-dimensional slot flow in the study of Sen and David could be considered. Figure 3 shows the comparison for the free surface in the case of a slot with an aspect ratio of 0·2 (Figure 9 in Reference 34). The input data are according to those of Sen and David, i.e. Marangoni number = 1, capillary number = 5, Reynolds number = 5 and Biot number = 1. As shown, the agreement is very good, considering the fact that the asymptotic solution itself is an approximation.

Negative $\partial\gamma/\partial T$

Calculations were made for stationary weld pools of 6061 aluminium produced by a power source of 1800 W. The power density distribution was assumed Gaussian with an effective radius of 4 mm.

The surface tension versus temperature relationship shown by the solid line in Figure 4 is for pure aluminium[35] and was used here as an approximation merely for computational purposes rather than for comparison with experimental results. It is however recognized that alloying elements in aluminium can have a significant effect on its surface tension, but not as much

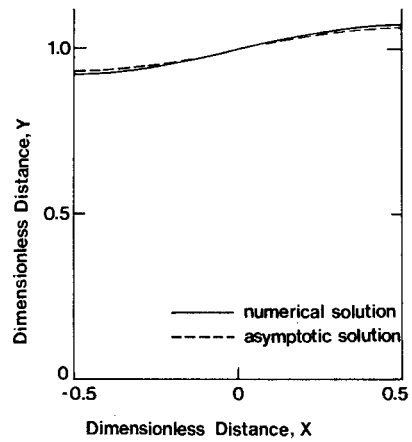

Figure 3. Surface geometry of a fluid between a hot wall (left) and a cold wall (right). Numerical solution from the present study (solid line) versus asymptotic solution from Sen and David[34] (broken line)

on its surface tension temperature coefficient. The solid line in Figure 4 has a slope $\partial\gamma/\partial T$ of $-0{\cdot}35\times10^{-3}\,\mathrm{kg\,s^{-2}\,°C^{-1}}$. Like pure aluminium, most pure metals have a negative $\partial\gamma/\partial T$.

The calculated temperature and velocity fields due to the Marangoni convection with $\partial\gamma/\partial T=-0{\cdot}35\times10^{-3}\,\mathrm{kg\,s^{-2}\,°C^{-1}}$ are shown in Figure 5(a). The deformation of the weld pool surface due to Marangoni convection is such that the weld pool surface is depressed near the centre but elevated near the edge. An enlarged view of the velocity field is shown in Figure 5(b).

Figure 5(c) shows a portion of the orthogonal grid mesh in its final form. The grid spacing is very fine near the free surface in order to calculate Marangoni convection accurately, i.e. 5×10^{-6} mm or 5 μm. Also, the grid spacing is fine near the axis and the edge of the weld pool. Similar fine grid spacings near the pool surface have also been used by us for calculating Marangoni convection in weld pools with a rigid surface (e.g. References 4 and 7).

As shown in Figure 5(b), convection is rather strong at the weld pool surface but quickly diminishes below it over a thin layer of about 30 μm. Had the grid spacing been coarser, say 20 μm,

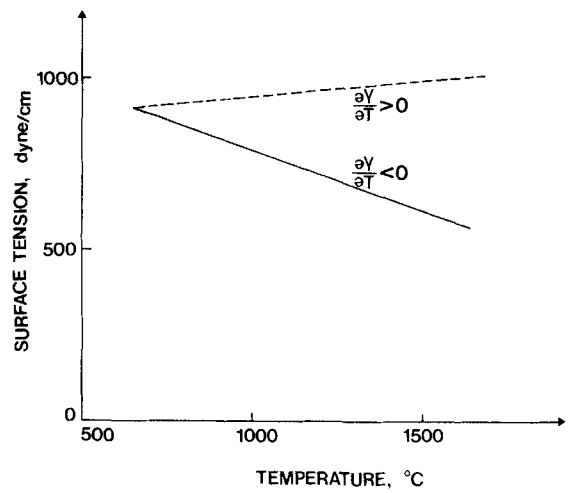

Figure 4. Surface tension versus temperature relationships used in the present study. The solid line is for pure aluminium[35] while the broken line is for an imaginary material

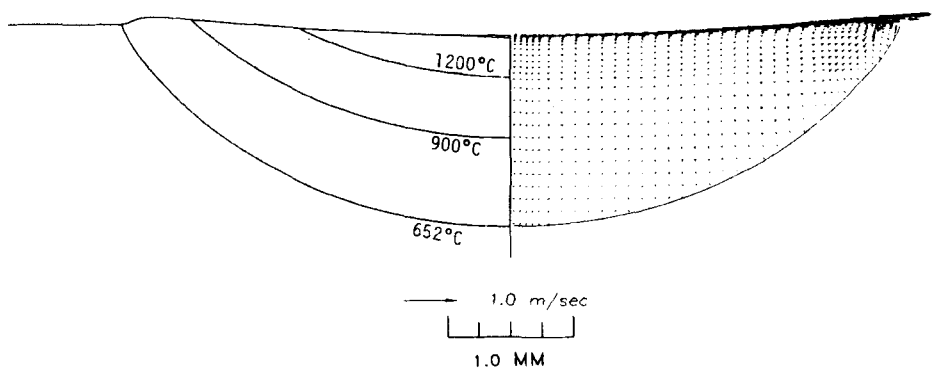

Figure 5(a)

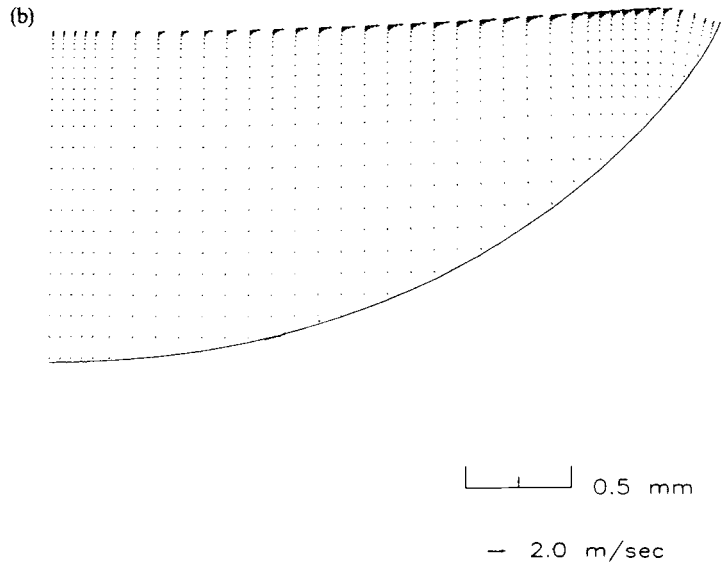

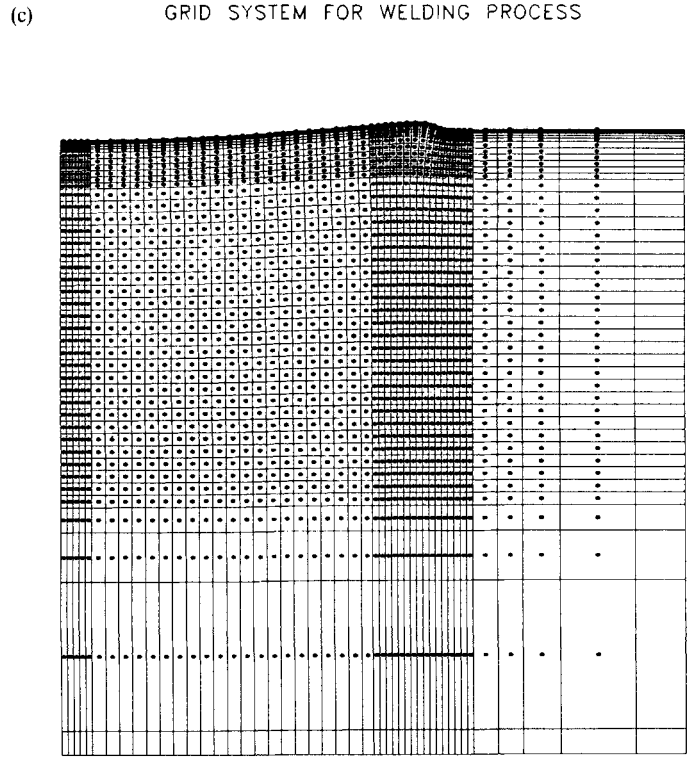

Figure 5. Calculated result for a deformable weld pool with a $\partial\gamma/\partial T$ of $-0{\cdot}35\times10^{-3}$ kg s^{-2} °C^{-1}: (a) temperature and velocity fields; (b) velocity field enlarged; (c) a portion of orthogonal curvilinear grid mesh used for computation. The maximum velocity, 1.8 m s^{-1}, is located along the pool surface at about 2·2 mm away from the centreline

the fluid flow calculation would have been inaccurate. The maximum surface velocity is about 1·8 m s^{-1} and occurs at around $r = 2{\cdot}2$ mm. Since the maximum surface velocity occurs rather close to the edge of the pool surface, the surface flow tends to push up the pool surface near the edge as it is being forced to stop at the edge.

In order to see the effect of weld pool surface deformation on heat transfer and fluid flow in the weld pool, the temperature and velocity fields in a similar weld pool but with a non-deformable surface are shown in Figure 6. As can be seen by comparing with Figure 5(a), the results are quite similar.

It should be mentioned that because of the rather high surface velocities, the Reynolds number might be high enough to make the flow unsteady to disturbances.[36, 37] In this respect the calculated velocity fields might not be exactly accurate in the quantitative sense.

Positive $\partial\gamma/\partial T$

In order to study the effect of the surface tension temperature coefficient $\partial\gamma/\partial T$ on the deformation of the weld pool surface, a positive value of $\partial\gamma/\partial T$ ($0{\cdot}1 \times 10^{-3}$ kg s^{-2} °C^{-1}) was used, as shown by the broken line in Figure 4.

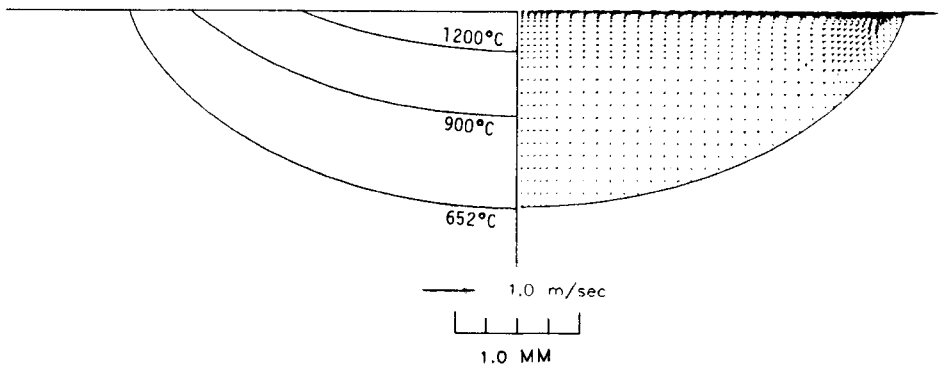

Figure 6. Temperature and velocity fields for a non-deformable weld pool with a $\partial\gamma/\partial T$ of $-0{\cdot}35 \times 10^{-3}$ kg s^{-2} °C^{-1}. The value and location of the maximum velocity are close to those in Figure 5

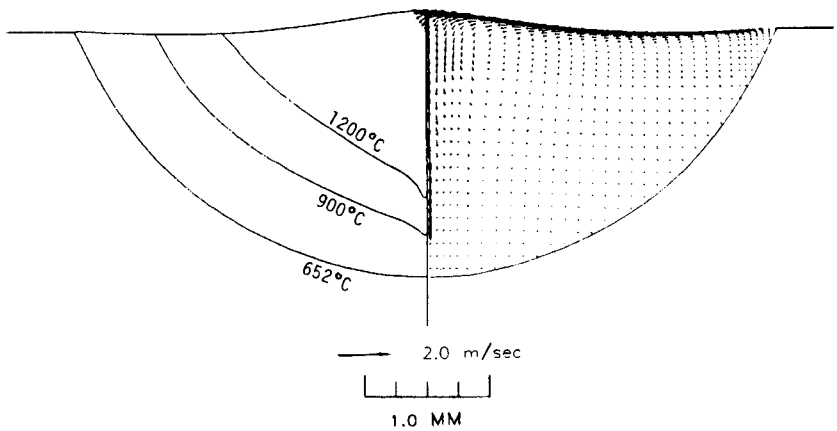

Figure 7(a)

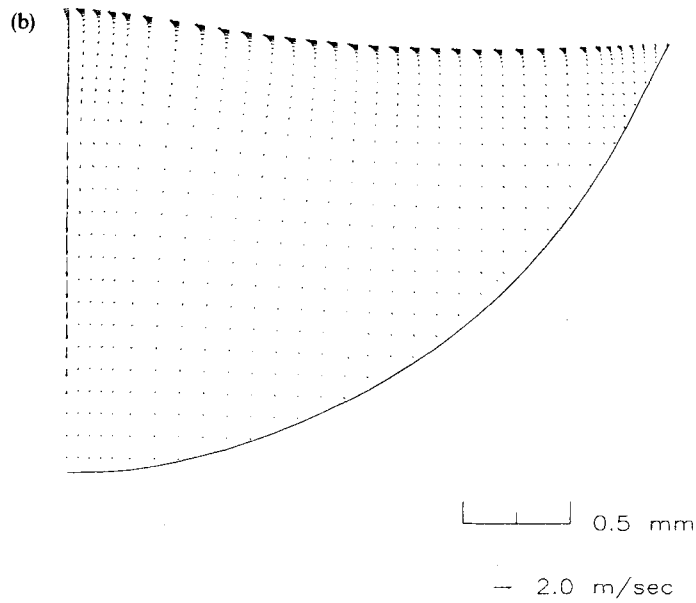

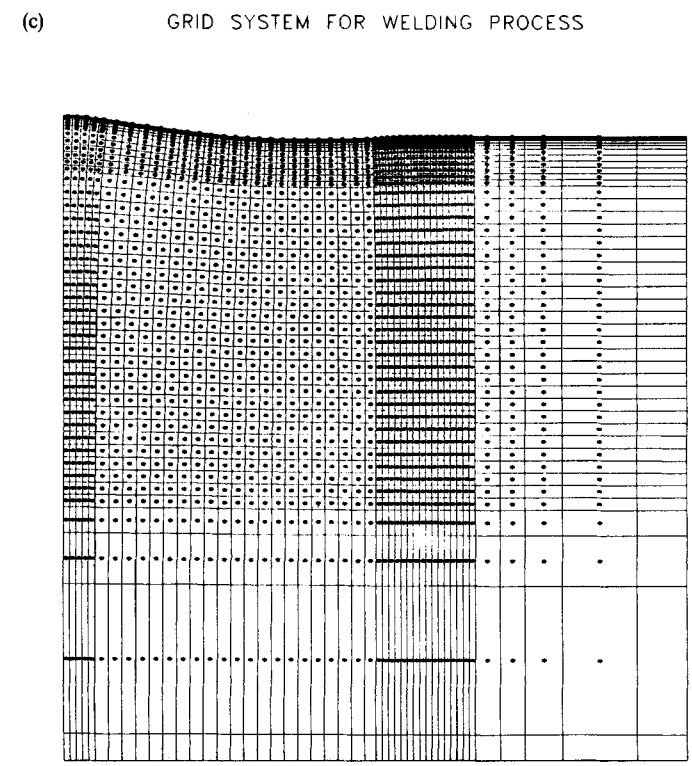

Figure 7. Calculated result for a deformable weld pool with a $\partial\gamma/\partial T$ of $0{\cdot}10 \times 10^{-3}$ kg s^{-2}°C^{-1}: (a) temperature and velocity fields; (b) velocity field enlarged; (c) a portion of orthogonal curvilinear grid mesh for computation. The maximum velocity, 2·3 m s^{-1}, is located along the centreline at about 1 mm below the free surface

The calculated temperature and velocity fields due to the Marangoni convection with $\partial\gamma/\partial T = 0{\cdot}1 \times 10^{-3}$ kg s^{-2} °C^{-1} are shown in Figure 7(a). An enlarged view of the velocity field is shown in Figure 7(b). A portion of the grid mesh in its final form is shown in Figure 7(c). It should be pointed out first that since the velocity vectors (V) are plotted at the positions of the dots in the grid mesh shown in Figure 7(c) and since the first column of dots is located not exactly along the centreline but slightly off it, the η-components of the velocity vectors near the top of this column are not zero. This should not be taken as failure to obey the boundary condition of $u = 0$ at the centreline. The fact that the fastest surface flow is closer to the centreline than to the edge of the weld pool explains the non-zero u mentioned above.

As shown in Figure 7(a), the centre of the weld pool surface is now slightly elevated while the outer portion is slightly depressed, i.e. the weld pool deformation is opposite to that for the Marangoni convection with $\partial\gamma/\partial T < 0$ (Figure 5(a)). This weld pool deformation is believed to be a result of the radially inward Marangoni convection induced by the positive value of $\partial\gamma/\partial T$.

As can also be seen by comparing Figure 7(a) with Figure 5(a), the pool depth is significantly greater with $\partial\gamma/\partial T > 0$. This is because the liquid metal at the free surface flows radially inwards to right under the arc, picks up the heat from the arc and then delivers the heat to the bottom of the pool. Consequently, the depth of the pool increases significantly.

Again, in order to see the effect of weld pool surface deformation on heat transfer and fluid flow in the weld pool, the temperature and velocity fields in a similar weld pool but with a non-deformable surface are shown in Figure 8. These fields can be compared with those shown previously in Figure 7(a). In both cases the axially downward velocities along the centreline of the weld pool decay as one moves away from the centreline. However, in the case of the deformed weld pool (Figure 7(a)) this decay is significantly more rapid. As a result, the isotherms in the deformed weld pool are pushed downwards almost only at the centreline, while those in the underformed weld pool are pushed downwards both at and in the vicinity of the centreline. In fact, the pool is about 14% deeper in the latter, suggesting that the pool depth can be significantly overestimated if the pool surface is assumed flat and non-deformable.

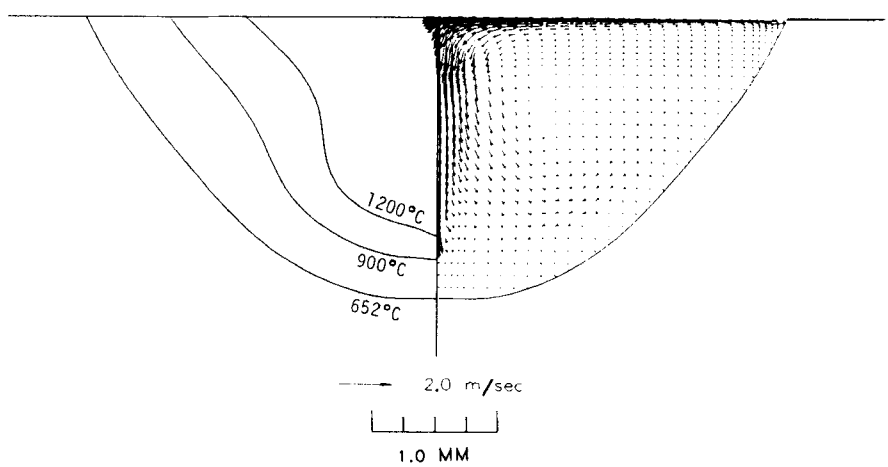

Figure 8. Temperature and velocity fields for a non-deformable weld pool with a $\partial\gamma/\partial T$ of $0{\cdot}10 \times 10^{-3}$ kg s^{-2} °C^{-1}. The value and location of the maximum velocity are close to those in Figure 7.

CONCLUSIONS

A steady-state two-dimensional model of heat transfer and fluid flow has been developed to describe the Marangoni convection in stationary weld pools. The present model differs from previous models in that the pool surface is unknown and is calculated with the help of orthogonal curvilinear co-ordinates.

The model agrees very well with the asymptotic solution of Sen and David[34] for Marangoni-convection-induced free surface geometry.

When the surface tension temperature coefficient $\partial\gamma/\partial T$ is negative, Marangoni convection is radially outwards, and the centre of the pool surface is depressed while the outer portion of the pool surface is elevated. When $\partial\gamma/\partial T$ is positive, the reverse is true.

In the case of a positive $\partial\gamma/\partial T$, the pool depth can be significantly overestimated if the pool surface is assumed flat.

ACKNOWLEDGEMENTS

The authors are grateful for the support of this study from the National Science Foundation under NSF Grant No. DMR 8419274. They also thank the reviewers for their helpful comments.

REFERENCES

1. G. M. Oreper, T. M. Eagar and J. Szekely, 'Convection in arc welding pool', *Welding J.*, **62**, 307s–313s (1983).
2. G. M. Oreper and J. Szekely, 'Heat and fluid flow phenomena in weld pools', *J. Fluid. Mech.*, **147**, 53–79 (1984).
3. C. Chan, J. Mazumder and M. M. Chen, 'A two-dimensional transient model for convection in laser melted pools', *Metall. Trans. A*, **15**, 2175–2184 (1984).
4. S. Kou and D. K. Sun, 'Fluid flows and weld penetration in stationary arc welds', *Metall. Trans. A*, **16**, 203–213 (1985).
5. S. Kou and Y. H. Wang, 'Weld pool convection and its effect', *Welding J.*, **65**, 63s–70s (1986).
6. S. Kou and Y. H. Wang, 'Three-dimensional convection in laser melted pools', *Metall. Trans. A*, **17**, 2265–2270 (1986).
7. S. Kou and Y. H. Wang, 'Computer simulation of convection in moving arc welds pools', *Metall. Trans. A*, **17**, 2271–2277 (1986).
8. Y. H. Wang and S. Kou, '3-D weld pool convection—a dimensionless presentation', in S. Kou and R. Mehrabin (eds), *Modeling and Control of Casting and Welding Processes*, The Metallurgical Society, Warrendale, PA, 1986, pp. 197–210.
9. S. M. Correa and R. E. Sundell, 'A computation and experimental study of the fluid flow in weld pools', in S. Kou and R. Mehrabian (eds), *Modeling and Control of Casting and Welding Processes*, The Metallurgical Society, Warrendale, PA, 1986, pp, 211–227.
10. C. L. Chan, R. Zehr, J. Mazumder and M. M. Chen, 'Three-dimensional model for convection in laser weld pool', in S. Kou and R. Mehrabian (eds), *Modeling and Control of Casting and Welding Processes*, The Metallurgical Society, Warrendale, PA, 1986, pp. 229–246.
11. J. Szekely, G. M. Oreper and J. Mckelliget, 'Heat and fluid flow phenomena in arc welding operations', in S. Kou and R. Mehrabian (eds), *Modeling and Control of Casting and Welding Processes*, The Metallurgical Society, Warrendale, PA, 1986, pp. 247–276.
12. J. Szekely, 'The mathematical modeling of arc welding operation', in S. A. David (ed.), *Advances in Welding Science and Technology*, ASM International, Metals Park, OH, 1986, pp. 3–14.
13. A. Paul and T. DebRoy, 'Heat transfer and fluid flow in laser melted weld pools', in S. A. David (ed), *Advances in Welding Science and Technology*, ASM International, Metals Park, OH, 1986, pp. 29–33.
14. R. E. Sundell, H. D. Solomon and S. M. Correa, 'Minor element effects on gas tungsten arc (GTA) weld penetration—weld pool physics', in S. A. David (ed), *Advances in Welding Science and Technology*, ASM International, Metals Park, OH, 1986, pp. 53–57.
15. Y. H. Wang and S. Kou, 'Driving forces for convection in weld pools', in S. A. David (ed), *Advances in Welding Science and Technology*, ASM International, Metals Park, OH, 1986, 65–69.
16. R. E. Craine, 'On determining the shape of weld pools', *Appl. Sci. Res.*, **44**, 261–275 (1987).
17. K. C. Tsao and C. S. Wu, 'Fluid flow and heat transfer in GMA weld pools', *Welding J.*, **67**, 70s–75s (1988).
18. M. P. Kanouff, 'Weld pool modeling', in R. W. Lewis, K. Morgan and W. G. Habashi (eds), *Numerical Methods in Thermal Problems, Vol. V, Part 1*, Pineridge Press, Swansea, 1987, pp. 15–26.
19. T. Zacharia, A. H. Eraslan and D. K. Aidun, 'Modeling of non-autogeneous welding', *Welding J.*, **67**, 18s–27s (1988).
20. T. Zacharia, A. H. Eraslan and D. K. Aidun, 'Modeling of autogeneous welding', *Welding J.*, **67**, 53s–62s (1988).

21. A. Paul and T. DebRoy, 'Prediction of Marangoni convection heat transfer and surface profiles during laser welding', in *Modeling and Control of Casting and Welding Processes IV*, The Metallurgical Society, Warrendale, PA, 1988, pp. 421–431.
22. R. McLay and G. F. Carey, 'Coupled heat transfer and viscous flow in weld pool analysis', *Int. j. numer. methods fluids*, **9**, 713–730 (1989).
23. M. C. Tsai and S. Kou, 'The advantages of orthogonal curvilinear coordinates in simulating Marangoni convection in deformed weld pools', in *Modeling and Control of Casting and Welding Processes IV*, The Metallurgical Society, Warrendale, PA, 1988, pp. 409–420.
24. L. E. Malven, *Introduction to the Mechanics of a Continuous Medium*, Prentice-Hall, Englewood Cliffs, NJ, 1969, pp. 641–672.
25. L. D. Landau and E. M. Lifshitz, *Fluid Mechanics*, 2nd Edn, Pergamon Press, Oxford, 1987, p. 241.
26. S. V. Patankar, *Numerical Heat Transfer and Fluid Flow*, Hemisphere, New York, 1980, pp. 88, 126.
27. W. M. Rohsenow and M. Y. Choi, *Heat, Mass and Momentum Transfer*, Prentice-Hall, New York, 1961, p. 523.
28. D. E. Schlinninger, I. G. Betz and H. Markus, 'Simplified determination of thermal experience in fusion welding', *Welding J.*, **49**, 410s–418s (1970).
29. M. L. Lin and T. W. Eagar, 'Effects of surface depression and convection in GTA welding', in S. A. David (ed.), *Advances in Welding Science and Technology*, ASM International, Metals Park, OH, 1986, pp. 47–51.
30. D. Rosenthal, 'Mathematical theory of heat distribution during cutting and welding', *Welding J.*, **20**, 220s–234s (1941).
31. M. C. Flemings, *Solidification Processing*, McGraw-Hill, New York, 1974, p. 35.
32. A. Thom and C. J. Apelt, *Field Computation in Engineering and Physics*, Van Nostrand, London, 1961, p. 130.
33. B. Carnahan, H. A. Luther and J. O. Wilkes, *Applied Numerical Methods*, Wiley, New York 1969, p. 73.
34. A. K. Sen and S. H. David, 'Steady thermocapillary flows in two-dimensional slots', *J. Fluid Mech.*, **121**, 163–186 (1982).
35. S. Z. Beer, *Liquid Metals*, Marcel Dekker, New York, 1972, Chap. 4.
36. P. M. Gresho and S. T. Chan, in *Proc. Fourth Int. Conf. on Numerical Methods in Laminar and Turbulent Flow*, Swansea, 9–12 July 1985.
37. H. S. Kheshgi and P. M. Gresho, 'Analysis of electron-beam vaporization of refractory metals', in *Electron Beam Melting and Refining—State of the Art*, Reno, NV, November 1986.